Microelectronics Reliability 139 (2022) 114831

Contents lists available at ScienceDirect

Microelectronics Reliability

journal homepage: www.elsevier.com/locate/microrel

Creep-fatigue lifetime estimation of efficient photovoltaic module ribbon interconnections

Alireza Eslami Majd [a,*], Nduka Nnamdi Ekere [b], Armin Rahmati Darvazi [c], Ali Amini Sedehi [d]

[a] School of Engineering, Faculty of Science and Engineering, University of Wolverhampton, UK
[b] Faculty of Engineering and Technology, Liverpool John Moores University, UK
[c] Faculty of Technology and Engineering, University of Guilan, Iran
[d] Department of Mechanical Engineering, University of Kashan, Iran

ARTICLE INFO

Keywords:
Efficient PV module interconnections
Solder joint
Creep-fatigue lifetime
Reliability

ABSTRACT

As the solar PV harvesting energy system are becoming more important sector of renewable energy day to day, improving the efficiency of the solar PV module and reducing the cost of modules are receiving more attentions of PV module manufacturers. Design of the PV module interconnection ribbons is one of the main focus for developing the efficiency of the PV modules and improving the reliability of the modules. In the last decade, new designs for the PV module interconnection ribbon have been introduced, however, there is still a need to optimize their configuration and geometry to achieve higher reliability without dropping the efficiency of the PV modules. Indeed, solely using the wider interconnection ribbons (to provide more joint length) may increase the reliability of the module, but it directly reduces the efficiency of module due to more shading effect. This study provides the results for determining the optimal design for long-term reliability of PV module interconnections. Three main PV module ribbon interconnection designs including Conventional Ribbon (CR), Light-Capturing Ribbon (LCR), and Multi-Busbar (MBB) interconnections are compared in terms of number of cycles to creep-fatigue failure. This study uses the FEM simulation and creep-fatigue reliability formulations to find the effect of the main geometrical parameters on the failure of different PV module ribbon interconnection designs. The finding showed that the MBB interconnections has up to 15 % higher creep-fatigue lifetime compared to the LCR and the CR interconnections.

1. Introduction

The rapid growth of solar PV cells has been driven by several factors, including the energy security and environmental concerns, the improving cost-competitiveness, and the growing demand for energy in developing and emerging economies where energy access remains a challenge. According to the IEA's latest 5-year forecast, renewable power capacity is set to expand by 50 % between 2019 and 2024, led by solar PV cell technologies [1]. Despite the global popularity and widespread use of solar PV modules, improving the performance and reliability of PV module designs remains a key challenge for the solar PV manufacturing sector, as manufacturer strive to satisfy their products' lifetime warranties.

The design of the PV module components involves achieving the best performance and the highest reliability and at the same time, saving the material consumptions and keeping the manufacturing cost low. Indeed, several performance parameters such as fill factor and power output of PV modules under damp heat-exposed and UV-aged tests are surveyed by researchers to find the effect of different designs and materials on the performance of the PV modules [2].

1.1. PV module ribbon interconnection

In a conventional PV module, the front-to-back cell interconnection technique is the most common cell connecting technique for generating suitable voltage to feed energy into the electrical power networks [4]. The front-to-back cell interconnection technique uses ribbon interconnections to connect the cells, and these ribbons are one of the key components of the PV module as it is widely known that over 40 % of PV module failures are linked to PV module interconnection solder failures [3]. The front-to-back cell interconnection technique also suffers the series resistance in the interconnection ribbon. This problem can be

* Corresponding author.
E-mail address: a.e.majd@wlv.ac.uk (A. Eslami Majd).

https://doi.org/10.1016/j.microrel.2022.114831
Received 23 August 2022; Received in revised form 7 October 2022; Accepted 13 October 2022
Available online 21 October 2022

effectively solved by using wider interconnection ribbons. However, using wider ribbons leads to high partial shading effect due to reflection of the incident rays from ribbon surface (about 2.3 % of the cell surface is covered by the conventional ribbon (CR)) and subsequently it results in more reduction of the short circuit current and the power output [5–7].

1.2. Efficient PV module ribbon interconnections

To solve the introduced challenges with shading effect interconnection ribbons for solar cell tabbing and subsequently the challenge with the efficiency of the system, there are new design of the interconnection ribbons such as Light Capturing/Harvesting Ribbon (LCR/LHR) and Multi-Busbar (MBB) which help to reduce the shading effect of ribbons on the cell. The LCR uses a grooved surface to reflect more light back onto the cell surface and improves the photocurrent recapture ratio of ribbon which causes an increase the power gain by 1.7 % [8]. Also, the roundness of the circular wire geometry in the MBB design assists to reflect the incident light from the ribbon surface onto the wafer surface and it makes less losing the received energy in comparison with the standard interconnection ribbons [9]. Besides, the MBB design uses high number of small round wires to decrease the busbar width and it results in an increase of the number of current paths to associate more uniform current distribution [10]. However, the MBB connector may suffer manufacturing errors associated with the non-homogeneity of solder coating around the copper-wire which results in earlier solder failure and crack (up to 21 %) [11,12]. Fig. 1 shows a schematic view of optical path and reflecting light from the interconnection back onto the cell surface for the designs using LCR and MBB interconnections compared to the CR interconnection.

1.3. The challenge

To understand the failure modes of the PV module including the failure mode of the PV module solder joint interconnections, investigation of the filed data could be the first step. However, the design based on the observation of failure modes in operation of the PV module, needs a long time equal to the service life the modules and this is not applicable as the manufacturers are motivated to introduce new designs with better performance and but with lower manufacturing cost. In terms of the reliability and failure mechanism of the PV module parts, particularly solder joints, the designs are not still sufficiently based on the available standards and more experimental and numerical analysis are needed to estimate the service life of the PV modules. To solve the challenge on better understanding of failure mechanism of different PV module components, the numerical analysis is the most available and is the lowest expensive way to find the failure behavior of crucial components such as PV module solder joint. These numerical analyses are mainly proposed to be implemented on the PV modules operating under service condition to find the lifetime of the components those massively affect the reliability of the whole PV module (in particular, PV module ribbon interconnections and solder joints). Therefore, the FEM study of main failure modes of crucial components (specially in case of the PV module solder joints, creep-fatigue failures) are required to achieve the exact results; and then to define the optimized designs.

The evaluation of creep-fatigue damage and the estimating the lifetime of the joint components have been widely studied from 1990s. However, there are still many introduced gaps of knowledge in facilizing the estimation techniques and methodologies for different material types and applications. For this, using new computing methods such as applying machine learning algorithms as well as FEM simulations have been developed to aid and speed up the evaluation of design parameters for a wide range of applications from microelectronics applications to heavy size structures [13–16]. This study investigates the creep-fatigue behavior of the solder joints used in the efficient PV module interconnection designs. For this purpose, the ABAQUS software package is used to implement the FEM models and the results from the FEM simulations are combined with the reliability terms (based on the creep strain energy models) to estimate the creep-fatigue life of the solder joints in each design. Also, a comparative study is presented to optimize the best PV module interconnection configuration in terms of high reliability and low material consumptions.

2. Methodology

The energy based models such as developed Morrow Energy Density model (based on the total strain energy density per cycle) have been developed in several works for estimating the creep-fatigue lifetime of solder joints [17,18]. In this approach, the experimental data and obtained the results of the FEM simulation are correlated to derive the formulation for prediction of the thermal creep fatigue life of SAC solder joints. Syed et al., developed a formula to estimate the number of cycles to creep-fatigue failure (N_f) for the solder joints operating under thermal cycling loads, as the following equation [19].

$$N_f = (W^{'} w_{acc})^{-1} \tag{1}$$

where W' is the energy density constant for failure (0.0019 for that SAC solder joints) and w_{acc} is the average accumulated creep energy density (per cycle). The average accumulated creep energy density for the solder joints is then given by the following equation:

$$w_{acc} = \frac{\sum W_i V_i}{\sum V_i} \tag{2}$$

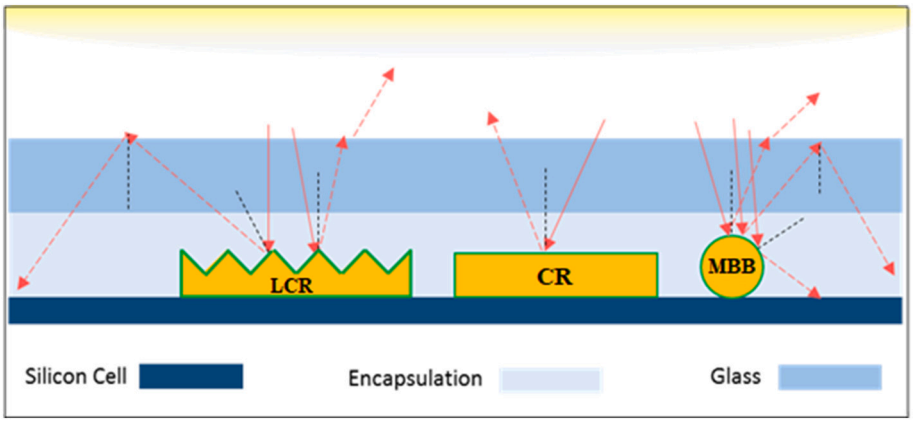

Fig. 1. Schematic views of optical path and reflecting light from different interconnections back onto the cell surface (left: the LCR, middle: CR and right: MBB interconnections). Continuous line shows the incident rays and the dashed lines shows the reflected rays.

where V_i and W_i are the element volume and the accumulated creep energy for each element, respectively.

In this study, to find V_i and W_i, the developed Morrow Energy Density model is used to determine the N_f. This model uses the stress–strain hysteresis energy loops for predicting the creep energy in each cycle. The strain-stress terms used in the models can be found by using the analytical constitutive models of creep behavior such as Hyperbolic Sine [19–21].

The Hyperbolic-Sine creep model in ABAQUS is used to find the total dissipated energy in the solder joint of LCR and MBB interconnections. Then, N_f of the solder joints are estimated by using the reliability formulation found by Syed et al. [19]. The Hyperbolic-Sine creep model is one of the most famous constitutive models to evaluate the elastic plastic creep behavior, as it considers temperature and strain rate dependency of the material properties [22]. Eq. (1) shows the formula to express Hyperbolic-Sine creep model; and the related parameters and the values for the SAC solder joint materials are shown in Table 1.

$$\dot{\varepsilon}_{cr} = A(sinh(\beta\sigma))^{n} exp\left(-\frac{Q}{RT}\right) \quad (3)$$

2.1. Validation of the approach

To validate the present methodology for creep-fatigue investigation, the results from the simulation of SAC solder joint in Wafer Level Chip Scale Packages (WLCSP) are compared with the literature [24–26]. For this, the 2D and 3D FEM simulation models for the WLCSP under operating a standard thermal cycling load (with temperature ranging between −40 °C and 125 °C during 15 min, and 10 min dwell time) are considered to find the best simulation approach in terms of the running speed and the accuracy of results. The package size is 132 × 77 × 1 mm, and the diameter, pitch and height of solder joints are 0.25 mm, 0.4 mm and 0.166, respectively (see Fig. 2) [24].

Fig. 3 compares the FEM results for 2D and 3D models (from this study) with the results from the literatures [24,25]. As Fig. 3 shows, the corners of solder joint in contact with the chip has the maximum creep strain and creep dissipated energy density where is reported as nucleation of the crack [26].

Table 2 compares estimated N_f using the present methodology with the N_f reported in the literatures. As Table 2 shows, there are good agreements between the estimated lifetime using the present methodology in this study and the experimental lifetime. The results show that 3D modelling provides more accuracy (6 % error) compared to 2D modelling (9.8 % error). The main reasons for the errors can be uncertainties in considering the constant material properties for the solder joints, in addition to the consideration of more simplifications in the geometry of model and load fluctuation Furthermore, the higher error of the 2D modelling could be because the used creep-fatigue lifetime model parameters in the present methodology have been determined based on the investigation of the 3D FEM models. However, the geometry of solder joint in the PV module interconnection is very simpler than the geometry of solder joint in the WLCSP, and the cross-section of solder joint in the PV module interconnection is same for each slice of the model. So, it should be expected that using the 2D FEM model for the solder joint in the PV module interconnection can have less errors rather than the solder joints in the WLCSP. Although the results show that using the 3D model can provide more accurate estimated lifetime, there is still a convincing accuracy for the estimation of lifetime using the 2D model. I t should be also mentioned that using the 2D model for the simulation has reduced the computing time about 85 % compared to the 3D model. Hence, the 2D models used in this study can reasonably predict the creep-fatigue life of the PV module solder interconnection.

Table 1
Parameters of the Hyperbolic-Sine creep model and the values for SAC solder joint material [23].

Symbol	Parameter	Unit	Value
$\dot{\varepsilon}_{cr}$	Scalar creep strain rate	Sec. $^{-1}$	Found during analysis
A	Boltzmann's constant	J/K	1.381×10^{-23}
β	Constant	MPa^{-1}	0.02447
n	Constant	–	6.41
σ	Von Mises effective stress	MPa	Found during analysis
R	Gas constant	$J{\cdot}Mol^{-1}{\cdot}K^{-1}$	8.314
Q	Activation energy	$J{\cdot}Mol^{-1}$	6500 × R
T	Absolute temp.	K	Changing during analysis

3. FEM modelling

3.1. PV module ribbon interconnection dimensions

Table 3 summarizes the design parameters for the investigated LCR and MBB interconnections in this section. As Table 3 introduces seven 2-cases for the LCR and MBB interconnections to be compared for finding effect of the LCR width, the MBB diameter on the number of cycles to creep-fatigue failure (N_f). The required number of ribbons is also considered to have same cross-section area for both ribbon interconnection types. For example, the case number #1 for MBB interconnection uses 15 ribbons with 276 μm diameters ($0.9mm^2$ cross-section area) which is comparable with the LCR interconnection with 5 ribbons and 900 μm ribbon width. The maximum thickness of the LCR interconnections presented in Table 3 is considered 250 μm (the average thickness is 200 μm). Also, the solder thickness for both LCR and MBB interconnection are assumed 20 μm and the silver-pad thicknesses are 40 μm and 20 μm for the LCR and MBB interconnection, respectively.

3.2. Material properties

The metallic materials used in this study are assumed with elastic-plastic behavior and the details of the mechanical properties of the materials are from the previous work [27] (see Tables 4 and 5). For a more realistic simulation, the temperature dependency of PV module materials used in the present FEM simulations are considered and they include temperature dependency of the CTE for copper, silver, aluminum, SAC solder joint and silicon, and the temperature dependency of the Young's Modulus and Plastic Stress for solder joints [27].

3.3. Load condition

To simulate the PV module operating under thermal cycling creep-fatigue condition, the models are subjected to a homogenous thermal cycling load, with time history in accordance with the IEC 61215-2:2016 standard (see Fig. 4) [28]. For this study, a minimum temperature of -40 °C and a maximum temperature of the 85 °C are considered for the thermal cycles. The cycles start at ambient temperature (25 °C) and then the minimum temperature is experienced after cooling the module with a rate of 100 °C per hour and then the temperature remains constant for 10 min (dwelling time). Following this, with a similar heating up rate (100 °C per hour), the temperature increases to jump up to 85 °C and again it remains without any change for another 10 min. After staying 10 min at the highest temperature of the cycle, the model starts to cool down to reach the ambient temperature and to finish the cycle and then immediately the second cycle starts with the same temperature oscillating of the first cycle.

3.4. Elements and boundary conditions

In this study, to increase the computational solution speed, 2D models (using four-node bilinear plane strain quadrilateral, CPE4) are considered for the simulation of the PV module interconnections due to high ratio of the interconnection length to the other dimensions of model. Also, the symmetry boundary condition is applied to the mid-

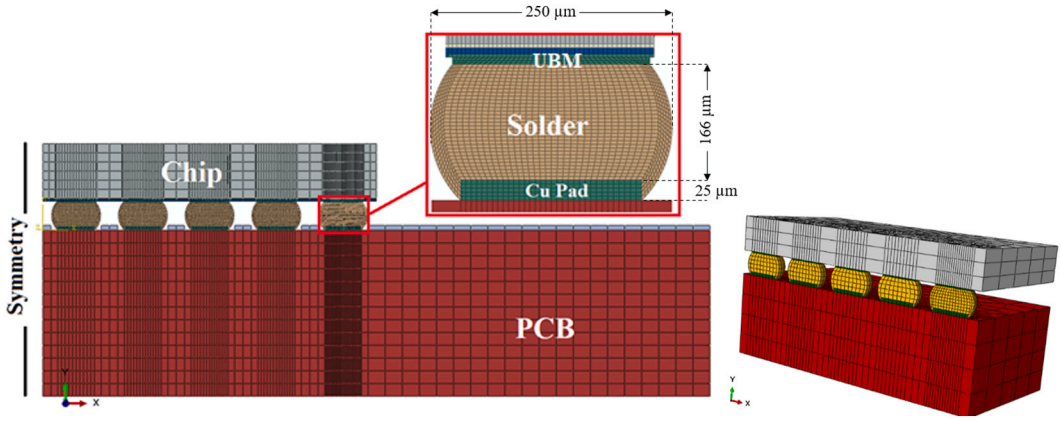

Fig. 2. FEM view of the WLCSP model used for the validation of creep-fatigue analysis, Right: 2D FEM model, Left: 3D FEM model (symmetry in Z direction).

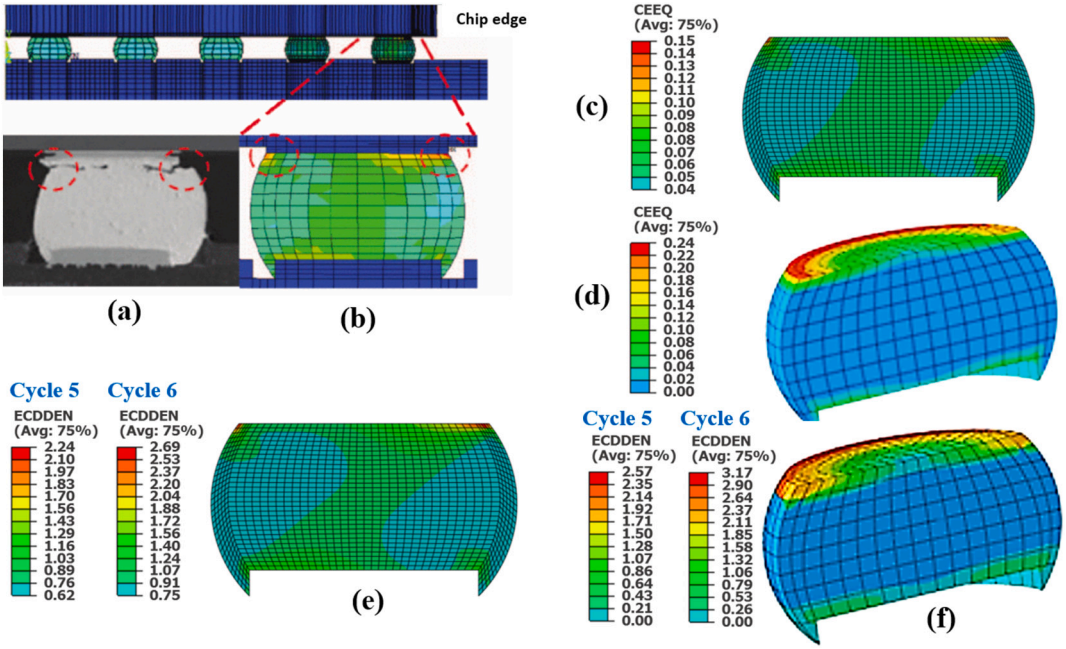

Fig. 3. (a) Observed failure due to crack in solder joint from experiment [26], (b) equivalent creep strain after cycle 5 (CEEQ) in the corner solder joint of WLCSP, from previous 2D model [25], (c) CEEQ, from the present 2D model, (d) CEEQ, from the present 3D model, (e) total creep dissipated energy density (ECDDEN, in mJ/mm^3) after cycle 5 and 6 from the present 2D model, and (f) ECDDEN from the present 3D model.

Table 2
Lifetime model parameters and estimated N_f for the solder joint in WLCSP.

Lifetime model parameter $N_f = C(w_{acc})^{\eta}$	FEM simulation [25]	FEM simulation [24]	Present 3D FEM simulation	Present 2D FEM simulation
w_{acc} (from FEM)	0.35	0.39	0.49	0.44
C	145	175	526	526
η	−2	−1.9	−1	−1
N_f	1152	1058	1074	1112
N_f from experiment [26]: 1013				
Error for the N_f	13.7 %	4.4 %	6 %	9.8 %

points of the ribbon interconnection section and bottom-end of the Tedlar material is fixed in thickness direction. Fig. 5 shows the FEM views of the simulated MBB and LCR interconnections studied in this work, showing the applied boundary conditions, meshing style and the arrangement of component materials.

Table 3
Dimensions and numbers of the LCR and MBB ribbon interconnections for the creep-fatigue analysis.

Case number	MBB interconnection			LCR interconnection		
	Ribbon diameter (µm)	Ribbons numbers	Cross-section Area (mm^2)	Ribbon width (µm)	Ribbons numbers	Cross-section area (mm^2)
1	276	15	0.90	900	5	0.90
2	291	15	1.00	1000	5	1.00
3	306	15	1.10	1100	5	1.10
4	319	9	0.72	1200	3	0.72
5	332	9	0.78	1300	3	0.78
6	345	9	0.84	1400	3	0.84
7	357	9	0.90	1500	3	0.90

Table 4
Mechanical Properties of material used in the FEM simulation of PV module interconnection [27].

	IMC	Solder (SAC)	Silver	Al	Copper	EVA	Silicon	Tedlar	Glass
Elastic modulus (GPa)	110	See Table 5	69	68.3	121	11	130	2.138	73.0
Poisson's ratio	0.3	0.35	0.365	0.34	0.34	0.499	0.28	0.4	0.235
Yield Stress (MPa)	–	–	43	85	121	12	170	41	–
Thermal expansion coefficient (ppm/K)	See Table 5	See Table 5	See Table 5	See Table 5	See Table 5	270	See Table 5	78	8.0
Plastic stress (MPa) @ strain	–	See Table 5	43@0.001120@0.04	85@0.001100@0.12	121@0.001217@0.01234@0.02248@0.04	–	–	41@0.0055@0.9	–

Table 5
Temperature dependency of the material properties used in the FEM simulation [27].

Temp. (°C)	Interpolated data for the coefficient of thermal expansion (ppm/K)						Young's modulus (GPa)	Yield stress (MPa)	Plastic stress (MPa) at 0.065 strain
	Copper	Silver	Al	Silicon	IMC	Solder	Solder		
0	16.22	18.67	22.50	2.35	17.7	21.3	49	71	145
30	16.60	18.98	23.29	2.63	18	21.81	46.9	52	131
60	16.91	19.20	23.85	2.87	18.3	22.32	44.8	16	110
90	17.22	19.42	24.41	3.04	18.6	22.83	42.7	–	–
120	17.53	19.65	24.97	3.20	19	23.34	40.6	–	–
150	17.76	19.91	25.40	3.36	19.8	23.85	38.5	–	–

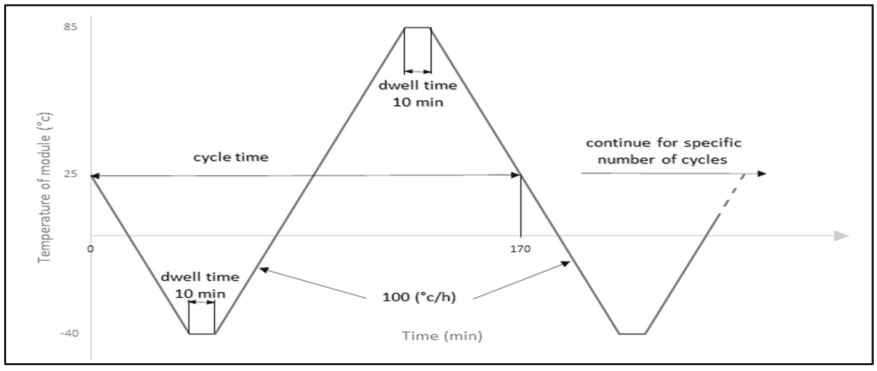

Fig. 4. Applied thermal cycle amplitude in accordance with the IEC 61215-2:2016 [28].

4. Results and discussion

4.1. Number of cycles to creep-fatigue failure

To find the effect of the LCR and the MBB geometry design on the number of cycles to creep-fatigue failure (N_f), several FEM cases (presented in Table 2) are simulated and investigated operating under thermal cycling condition with temperature ranging from −40 °C to 85 °C.

Fig. 6 compares the value of N_f for the LCR and MBB designs presented in Table 3. It is seen that the MBB interconnection designs can provides higher reliability compared to the LCR interconnection designs due to having higher N_f (10 % to 15 % higher). Also, as Fig. 6 suggests, the samples number #1 has higher N_f rather than other samples, which means that using the MBB interconnection with 15 ribbons with diameter of 276 μm; and also using a design with 5 LCR interconnections with 900 μm width can provide more reliability. However, the LCR interconnections with 1000 μm width (sample number #2) can be also suggested as it provides almost same N_f, and it provides more cross-section area compared to the sample number #1; and this means that there is less electrical resistance in the ribbon designed based on the sample number #2. Similarly, to have consistency in the cross-section areas of ribbons, the MBB interconnection sample number #2 (with diameter of 291 μm) is selected for finding the effect of geometrical parameters on the creep-fatigue lifetime of different PV module ribbon interconnection designs.

4.2. Effect of solder and copper thickness

Fig. 7 shows the effect of solder thickness and also copper (Cu) thickness on the value of N_f for the LCR interconnection deigns using 5 ribbons with 1000 μm width and 40 μm silver-pad thickness. The results show that an increase in the solder joint thickness leads to a slight increase in N_f (up to 5 %). In addition, Fig. 7 shows that increasing the copper thickness leads to a decrease in N_f, in which the LCR interconnection with 150 μm average copper thickness provides about 6 % higher N_f, when it is compared to the LCR interconnection with 200 μm average copper thickness. The results shown in Fig. 7 suggests that a LCR

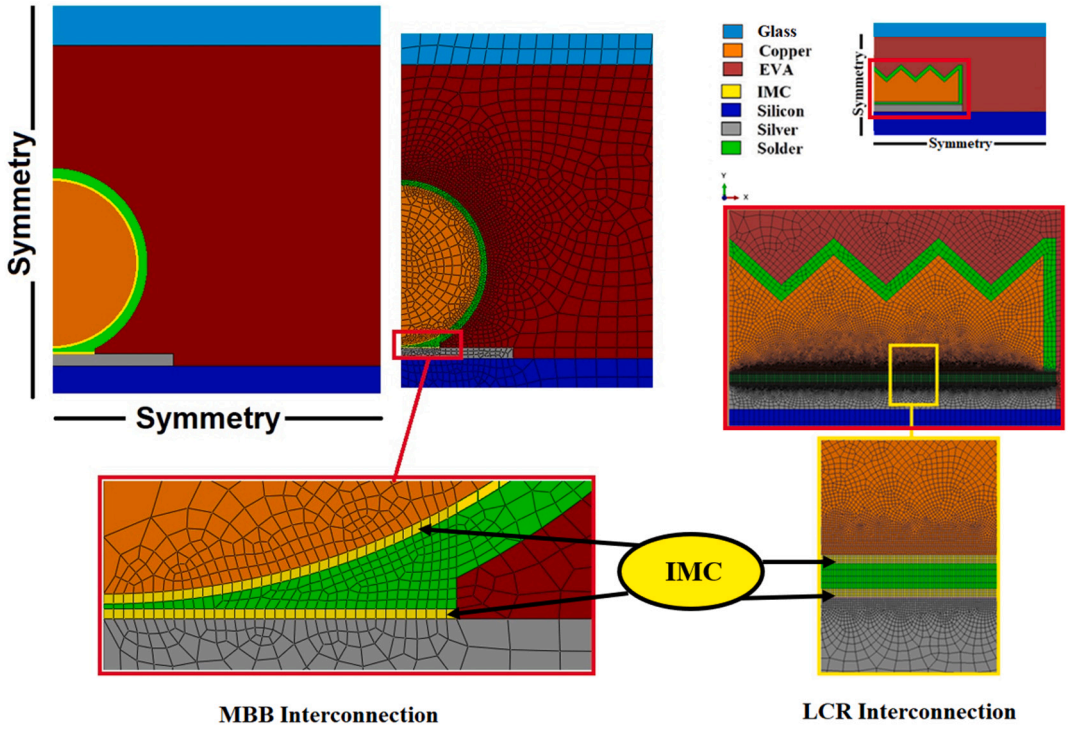

Fig. 5. FEM views of the MBB (left) and the LCR (right) PV module interconnections.

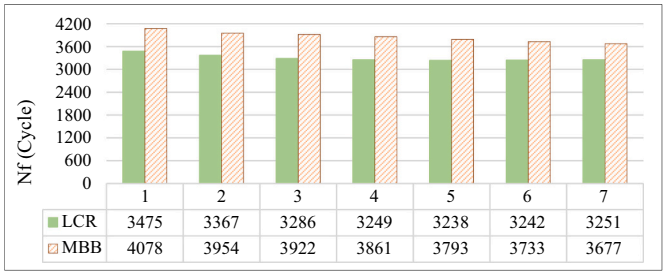

Fig. 6. Number of cycles to creep-fatigue failure (N_f) for different LCR and MBB interconnection designs with same cross-section areas, but with different ribbon width/diameter and numbers.

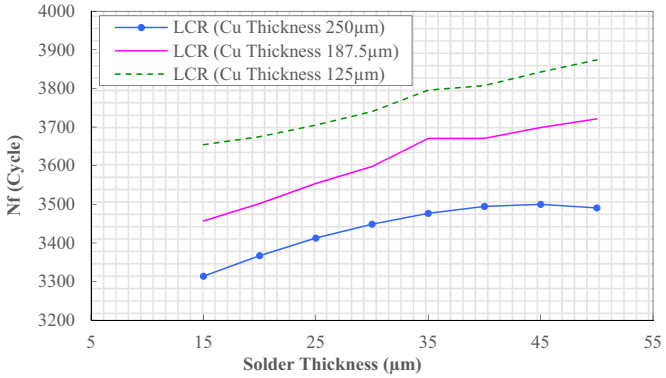

Fig. 7. Effect of solder and copper (Cu) thickness on N_f for the LCR interconnection.

interconnection with 20 μm solder joint thickness and 150 μm average copper thickness can be an optimal design as this configuration provides high value of N_f (3850 cycles), but it remarkably saves the material consumptions. This finding is consistent with the results obtained for the cracking parameters in the previous work [29].

4.3. *Effect of silver-pad thickness and solder thickness*

Fig. 8 shows the effect of silver-pad thickness on the associated N_f for the LCR and MBB interconnections with 20 μm solder thickness. Average copper thickness of the LCR interconnection and ribbon diameter of the MBB interconnection are considered 150 μm and 291 μm, respectively. It is shown that increasing the silver-pad thickness from 20 μm to 50 μm causes 32 % increase of N_f for the LCR interconnection. However, Fig. 8 suggests that there is no change of N_f when the silver-pad thickness of the MBB interconnection increases. To re-check the effect of solder thickness on the reliably of the MBB interconnection, the results of creep-fatigue analysis for the MBB interconnections with different solder joint thicknesses are presented in Fig. 9. As Fig. 9 shows, increasing the solder thickness results in an increase of N_f for the MBB interconnections, in which for the MBB interconnection with 40 μm silver-pad thickness, the increase of the solder thickness from 10 μm to 15 μm causes a significant increase in the N_f (166 %). However, for the MBB interconnection with solder thickness thicker than 15 μm, there is also a

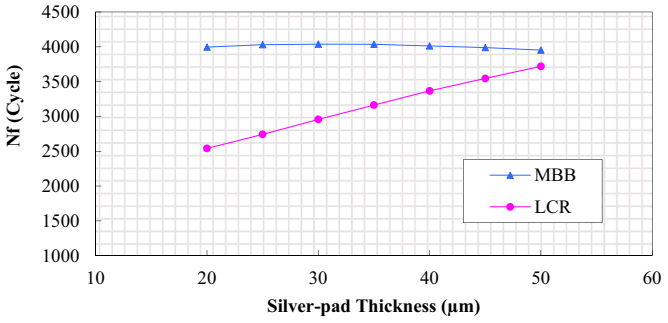

Fig. 8. Effect of silver-pad thickness on N_f for the LCR and MBB interconnections.

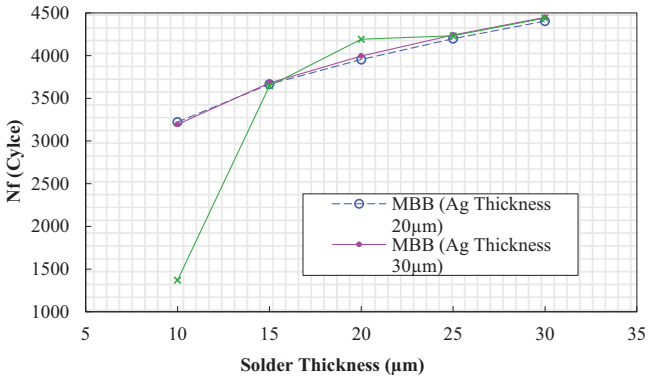

Fig. 9. Effect of solder thickness and silver-pad thickness on N_f for the MBB interconnection.

linear increase in N_f (up to 22 %) in which the N_f is not affected by the silver-pad thickness. Consequently, the MBB interconnection with 20 μm solder coating and silver-pad thickness can suggest more reliability for the PV module and also can help to save the material consumption.

4.4. Effect of initial crack on the N_f for selected PV module interconnection designs

According to the results for different studied PV module interconnection designs (namely: CR, LCR, and MBB interconnections), three configurations for each design are selected to be compared in terms of providing higher thermo-mechanical reliability. The selected configurations are based on reducing the solder and the silver consumptions in the designs, and at the same time providing relatively higher reliability of the interconnections. Furthermore, to consider the effect of initial cracks due to the high temperature lamination process (150 °C) (found from previous studies), N_f is calculated and compared for each selected designs with and without initial crack [12,27,29].

Table 6 shows dimensions of the selected PV module interconnection designs, and it also presents the high temperature crack specifications (crack initiation temperature and crack growth rate) and the calculated N_f (with and without considering the initial crack) for the selected PV module interconnection configurations. For instance, Table 6 presents that the best configuration for the CR interconnection uses 5 ribbons with the 900 μm ribbon width, the 200 μm copper thickness, the 20 μm solder thickness and the 40 μm silver-pad thickness. This configuration has $0.9mm^2$ cross-section area of the copper which helps to keep the electrical resistance low. As it is showed, this configuration exhibits a 18 μm initial crack length due to the high temperature lamination process, and the associated N_f is 3331 cycles.

As Table 6 indicates, using 5 LCR interconnections (LCR sample number #1) with 1000 μm ribbon width, with 150 μm average copper thickness, with 20 μm solder thickness and with 40 μm silver-pad thickness ($0.75mm^2$ total cross-section area of the copper) is recommended for the LCR interconnection, in which this configuration can endure the 3281 thermal cycles (with considering the initial crack). However, the LCR sample number #2 (with the 900 μm ribbon width and the 250 μm copper thickness, the total cross-section of copper is $0.9mm^2$) can be also recommended as this configuration exhibit lower electrical resistance, but still provided high N_f, 3114 cycles.

Table 6 shows that the CR interconnection shows less N_f affected by initial cracks compared to other designs, and the maximum effect of initial crack on N_f is on the LCR designs (10.4 % for sample number #2). However, Table 6 shows that the MBB interconnection has higher N_f (up to 15 %) compared to the CR and the LCR interconnection designs (i.e. higher thermal creep-fatigue lifetime). It is found that the MBB sample number #1 and #2 (with 15 ribbons, with 20 μm solder thickness with 20 μm silver-pad thickness, and with 291 μm and 276 μm copper diameters, respectively) provide much higher N_f (3813 and 3808 cycles, respectively) compared to the sample number #3 with 15 μm silver-pad thickness (with N_f of 3380 cycles).

5. Conclusion

This study considered three main PV module interconnection designs (Conventional Ribbon (CR), Light-Capturing Ribbon (LCR), and Multi-Busbar (MBB) interconnections) to find the effect of different geometrical parameters (namely: solder thickness, silver pad thickness, copper thickness, and ribbon width) on the number of cycles to creep-fatigue failure, N_f.

For each interconnection designs, the FEM simulation and the creep-fatigue reliability formulation were used to define the best three configurations in terms of using less the solder and the silver material, and also providing higher N_f for long-term reliability of PV module interconnections.

The effect of initial cracks in the solder joint (due to high temperature lamination process) on N_f was also considered to define the optimal design and configuration. The results showed that the N_f of CR interconnection is less affected by initial cracks compared to other designs, and the maximum effect of initial crack on N_f is for the LCR designs (10.4 %).

The results suggested that using 5 LCR and CR interconnections with 900-1000 μm ribbon width, with 20 μm solder thickness and with 40 μm silver-pad thickness and with copper thickness of 200 μm and 150 μm (for LCR and CR, respectively), relatively provide the best configuration for theses interconnection designs.

The results suggested that the MBB interconnections can provide more thermo-mechanical reliability compared to the LCR and the CR interconnection designs (up to 15 %), and the MBB interconnection with 15 ribbons, with 291 μm and 276 μm copper diameters, with 20 μm solder thickness and with 20 μm silver-pad thickness has higher

Table 6
Dimensions, initial crack specification, and the N_f for the selected PV module interconnection designs.

Designs		CR			LCR			MBB		
Geometrical parameters		1st	2nd	3rd	1st	2nd	3rd	1st	2nd	3rd
Number of ribbons		5	5	3	5	5	5	15	15	15
Ribbon width (μm)		900	1000	1200	1000	900	1000	291	276	276
Ave. copper thickness (μm)		200	200	200	150	200	100	291	276	276
Solder thickness (μm)		20	20	20	20	20	20	20	20	15
Silver-pad thickness (μm)		40	40	40	40	40	40	20	20	20
Copper area (mm^2)		0.9	1	0.72	0.75	0.9	0.5	1	0.9	0.9
Crack initiation temp. (°C)		98	102	104	87	69.5	106	98	102	110
Crack growth rate (μm/°C)		0.35	0.45	0.6	0.5	0.58	1	0.1	0.19	0.25
Initial crack length at 150 °C (μm)		18	22	28	31.5	46.69	44	5	9	10
N_f (cycle) T: −40 °C to 85 °C	W.O. crack	3471	3334	3205	3502	3475	3369	3954	4078	3644
	With crack	3331	3190	3058	3281	3114	3073	3813	3808	3380
	Effect (%)	4.0	4.3	4.6	6.3	10.4	8.8	3.6	6.6	7.2

reliability compared to all studied designs.

CRediT authorship contribution statement

Alireza Eslami Majd: Conceptualization, Methodology, Resources, Software, Formal analysis, Validation, Original draft preparation, Writing- Reviewing and Editing

Nduka Nnamdi Ekere: Supervision, Project administration

Armin Rahmati Darvazi: Data curation, Visualization, Formal analysis

Ali Amini Sedehi: Writing- Reviewing and Editing, Software, Validation

Declaration of competing interest

The authors declare that they have no known competing financial interests or personal relationships that could have appeared to influence the work reported in this paper.

Data availability

Data will be made available on request.

Acknowledgment

The authors would like to acknowledge the support of the Faculty of Science and Engineering, University of Wolverhampton for providing the sponsorship for the corresponding author's Ph.D. study.

References

[1] IEA Renewables 2019, Paris, 2019.
[2] E. Wang, H.E. Yang, J. Yen, S. Chi, C. Wang, Failure modes evaluation of PV module via materials degradation approach, Energy Procedia 33 (2013) 256–264.
[3] F.P. McCluskey, Reliability modeling for photovoltaic modules, Available at:&lt, in: NREL Photovoltaic Module Reliability Workshop, Denver, Colorado, 2010, Http://Www1.Eere.Energy.Gov/Solar/Pdfs/Pvrw2010_mccluskey.Pdf. (Accessed 12 April 2012).
[4] S. Wiese, F. Kraemer, N. Betzl, D. Wald, Interconnection technologies for photovoltaic modules-analysis of technological and mechanical problems, in: 2010 11th International Thermal, Mechanical & Multi-Physics Simulation, and Experiments in Microelectronics and Microsystems (EuroSimE), IEEE, 2010, pp. 1–6.
[5] E.M. Sachs, J. Serdy, A.M. Gabor, F. van Mierlo, T. Booz, Light-capturing interconnect wire for 2% module power gain, in: Proc. 24th EU PVSEC, Hamburg, Germany, 2009, pp. 3222–3225.
[6] S. Pareek, N. Chaturvedi, R. Dahiya, Optimal interconnections to address partial shading losses in solar photovoltaic arrays, Sol. Energy 155 (2017) 537–551.
[7] R. Ramaprabha, B.L. Mathur, A comprehensive review and analysis of solar photovoltaic array configurations under partial shaded conditions, Int. J. Photoenergy 2012 (2012).
[8] I. Chung, H. Oh, U. Baek, N. Yoon, W. Lee, E.-C. Cho, I.-S. Moon, H.Young Son, Light capturing film on interconnect ribbon for current gain of crystalline silicon PV modules, in: 2013 IEEE 39th Photovoltaic Specialists Conference (PVSC), IEEE, 2013, pp. 1478–1480.
[9] S. Braun, G. Micard, G. Hahn, Solar cell improvement by using a multi busbar design as front electrode, Energy Procedia 27 (2012) 227–233.
[10] J. Schneider, M. Turek, M. Dyrba, I. Baumann, B. Koll, T. Booz, Combined effect of light harvesting strings, anti-reflective coating, thin glass, and high ultraviolet transmission encapsulant to reduce optical losses in solar modules, Prog. Photovolt. Res. Appl. 22 (2014) 830–837.
[11] J. Walter, M. Tranitz, M. Volk, C. Ebert, U. Eitner, Multi-wire interconnection of busbar-free solar cells, Energy Procedia 55 (2014) 380–388.
[12] A. Eslami Majd, N.N. Ekere, Numerical analysis on thermal crack initiation due to non-homogeneous solder coating on the round strip interconnection of photovoltaic modules, Sol. Energy 194 (2019), https://doi.org/10.1016/j.solener.2019.10.092.
[13] H.H. Gu, R.Z. Wang, S.P. Zhu, X.W. Wang, D.M. Wang, G.-D. Zhang, Z.C. Fan, X.C. Zhang, S.T. Tu, Machine learning assisted probabilistic creep-fatigue damage assessment, Int. J. Fatigue 156 (2022), https://doi.org/10.1016/j.ijfatigue.2021.106677.
[14] R.Z. Wang, H.H. Gu, S.P. Zhu, K.S. Li, J. Wang, X.W. Wang, M. Hideo, X.C. Zhang, S.T. Tu, A data-driven roadmap for creep-fatigue reliability assessment and its implementation in low-pressure turbine disk at elevated temperatures, Reliab. Eng. Syst. Saf. 225 (2022), https://doi.org/10.1016/j.ress.2022.108523.
[15] V. Samavatian, M. Fotuhi-Firuzabad, M. Samavatian, P. Dehghanian, F. Blaabjerg, Iterative machine learning-aided framework bridges between fatigue and creep damages in solder interconnections, IEEE Trans. Compon. Packag. Manuf. Technol. 12 (2022) 349–358, https://doi.org/10.1109/TCPMT.2021.3136751.
[16] Y. Xu, J. Xian, S. Stoyanov, C.J. Bailey, R. Coyle, C. Gourlay, F.P.E. Dunne, A multi-scale approach to microstructure-sensitive thermal fatigue in solder joints, Int. J. Plast. 155 (2022), https://doi.org/10.1016/j.ijplas.2022.103308.
[17] J. Depiver, S. Malik, E.H. Amalu, Thermal fatigue life of Ball Grid Array (BGA) solder joints made from different alloy compositions, Eng. Fail. Anal. 125 (2021), https://doi.org/10.1016/j.engfailanal.2021.105447.
[18] F.K.A. Nyarko, G. Takyi, Life prediction in c-Si solar cell interconnections under in-situ thermal cycling in Kumasi in Ghana, Soldering Surf. Mt. Technol. 33 (2021) 215–223, https://doi.org/10.1108/SSMT-10-2020-0045.
[19] A. Syed, Accumulated creep strain and energy density based thermal fatigue life prediction models for SnAgCu solder joints, in: 2004 Proceedings. 54th Electronic Components and Technology Conference (IEEE Cat. No. 04CH37546), IEEE, 2004, pp. 737–746.
[20] H.U. Akay, Y. Liu, M. Rassaian, Simplification of finite element models for thermal fatigue life prediction of PBGA packages, J. Electron. Packag. 125 (2003) 347–353.
[21] P. Steinhorst, T. Poller, J. Lutz, Approach of a physically based lifetime model for solder layers in power modules, Microelectron. Reliab. 53 (2013) 1199–1202.
[22] E.H. Amalu, N.N. Ekere, Modelling evaluation of Garofalo-Arrhenius creep relation for lead-free solder joints in surface mount electronic component assemblies, J. Manuf. Syst. 39 (2016) 9–23.
[23] A. Schubert, R. Dudek, E. Auerswald, A. Gollhardt, B. Michel, H. Reichl, Fatigue life models for SnAgCu and SnPb solder joints evaluated by experiments and simulation, in: Electronic Components and Technology Conference 2003, IEEE, 1999, pp. 603–610.
[24] Y.C. Lee, K.N. Chiang, Reliability assessment of WLCSP using energy based model with inelastic strain energy density, in: 2019 International Conference on Electronics Packaging (ICEP), IEEE, 2019, pp. 329–332.
[25] C.Y. Tsou, T.N. Chang, K.C. Wu, P.L. Wu, K.N. Chiang, Reliability assessment using modified energy based model for WLCSP solder joints, in: 2017 International Conference on Electronics Packaging (ICEP), IEEE, 2017, pp. 7–15.
[26] M. Hsieh, S. Tzeng, Solder joint fatigue life prediction in large size and low cost wafer-level chip scale packages, in: 2014 15th International Conference on Electronic Packaging Technology, 2014, pp. 496–501, https://doi.org/10.1109/ICEPT.2014.6922704.
[27] A.Eslami Majd, N.N. Ekere, Crack initiation and growth in PV module interconnection, Solar Energy 206 (2020), https://doi.org/10.1016/j.solener.2020.06.036.
[28] IEC, Terrestrial Photovoltaic (PV) Modules – Design Qualification and Type Approval – Part 2: Test Procedures, 2016.
[29] A. Eslami Majd, N.N. Ekere, Study of high temperature crack initiation and growth in light capturing ribbon (LCR) PV module interconnection, Adv. Mater. Sci. Technol. 2 (2021), https://doi.org/10.37155/2717-526X-0202-3.